INSTITUTE OF PHYSICS PUBLISHING JOURNAL OF MICROMECHANICS AND MICROENGINEERING

J. Micromech. Microeng. **16** (2006) N23–N27 doi:10.1088/0960-1317/16/11/N02

NOTE

Investigation of a copper etching technique to fabricate metallic gas diffusion media

Feng-Yuan Zhang, Ajay K Prasad and Suresh G Advani

Fuel Cell Research Laboratory, Department of Mechanical Engineering, University of Delaware, Newark, DE 19711-3140, USA

E-mail: fyzhang@udel.edu

Received 13 June 2006, in final form 30 August 2006
Published 26 September 2006
Online at stacks.iop.org/JMM/16/N23

Abstract

A new fabrication technique based on etching is employed to convert a copper foil into a porous structure with an array of micron size pores. The motivation stems from the need to develop a more efficient and controllable gas diffusion medium for fuel cell applications. The influence of mask shape, mask width and etching time was investigated experimentally. A correlation to predict trench width with etching time was derived; normalizing by mask width allows one to collapse the data. The etching rates to obtain micro-scale features, which are of the order of 1–2 μm min^{-1}, are mainly dominated by the mask width due to mass-transport resistance. It is possible to control the pore dimensions, porosity and pore size distributions with this technique.

(Some figures in this article are in colour only in the electronic version)

1. Introduction

The PEM fuel cell (PEMFC) is a promising emerging technology for clean energy; however its cost has been one of the biggest barriers to date for its commercialization [1]. In addition, its performance and durability are significantly impacted by the characteristics of the gas diffusion medium (GDM) whose principal functions are to efficiently transport the reactants and products to and from the membrane, as well as to conduct heat and electric current [2]. Current GDM materials, which are primarily made of carbon fiber cloth or paper, have shown limited success. Their pore sizes and distribution are random and hence difficult to control. Moreover, during FC operation, carbon paper or cloth is normally under compressive stress, that reduces its thickness, and decreases the porosity and the permeability by up to 50% of its original value. This will also reduce the durability of the GDM and the fuel cell [3, 4]. Additionally, key issues of flooding and mass transport limitation under steady-state and transient (e.g., start-up) conditions demand novel morphology for carefully designing and controlling pore size distribution. It has also been shown that if the pores were straight and were not interconnected, the liquid water would freely drain out of GDM once the water flow was initiated [5–7]. Recently a mesh sheet with pores filled with electrically conductive powder and fluorine resin was introduced for FC applications. The inexpensive mesh sheet provided the mechanical support, while the powder was expected to enhance conductivity and transport. This variation met with limited success as it did not improve much on the areal weight, thickness and electric conductivity of the existing GDM; the permeability for both gas and liquid was low and it did not provide any control over its pore size and distribution [8].

With the rapid development of MEMS/nano technology, several solutions for improving thermal and electrical conductivity, mass transport and permeability are being explored. MEMS/nano technology provides advantages such as high precision, good repeatability and automated batch production [9]. In addition to silicon, micro/nano fabrication equipment can easily etch patterns with high feature resolution on metals with high thermal and electric conductivities, which are key functional requirements of the GDM in PEMFCs.

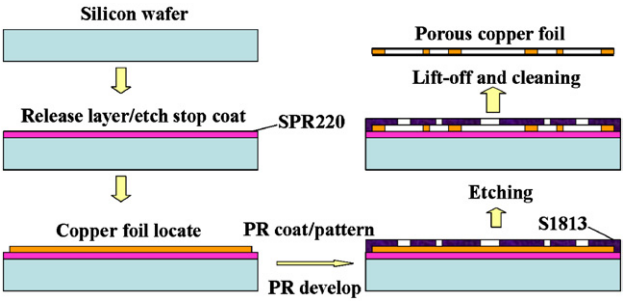

Figure 1. Fabrication process to convert a thin copper foil into a porous structure.

More importantly, wet etching provides a low-cost method, and it can result in a faithful transfer of the pattern on the underlying metal with the help of a patterned mask.

Copper has received considerable attention as a potential GDM material due to its lower cost, excellent thermal and electrical conductivity, its high resistance to electromigration, good durability and the potential to control the pore size density and distribution by masked etching. Etching rates of unmasked evaporated copper with etchants, and etchant concentrations were recently investigated [10, 11]. The etching rate of copper was also found to be hampered by the great disparity of grain orientations. Moreover, a recent study on etching morphology of single crystal copper suggested copper was etched by macro steps expending along a certain plane [12, 13]. Achieving the desired pattern requires careful mask design and control of several other factors such as the etchant, etching time, temperature and etching rate. In this work, wet isotropic etching of super thin copper (1 1 0) foil was performed. The effects of mask shape, mask width and etching time were experimentally investigated, and a normalized relation for the etched width with time was derived.

2. Experimental procedure

A novel gas diffusion medium was fabricated using 12.5 μm thick copper foil (Cu1 1 0). The extremely small thickness of the copper foil necessitates special care during processing as shown in figure 1. This special initial step consists of bonding the copper foil on to a standard silicon (Si) wafer by applying a sacrificial layer of photoresist material (SPR220) to the Si surface. To improve the adhesion of the sacrificial layer to both Cu and Si, the following two steps were performed. First, the Si wafer and copper foil were cleaned in a piranha solution (3:1 mixture of sulfuric acid and 30% solution of hydrogen peroxide) at room temperature for 10 min and dried, after which a hexamethyldisilazane (HMDS) layer was vapor coated on them for 15 min to promote adhesion with the sacrificial layer. A thick SPR220 photoresist layer was then applied on the Si wafer. To ensure a uniform thickness, the photoresist was spun on the wafer at an increasing speed from 0 to 3000 rpm for 30 s and subsequently at 3000 rpm for 20 s. The copper foil was then pressed on the photoresist SPR220 and baked at 100 °C for 30 s. These steps ensured that the copper foil could now be handled in a more robust manner, and subjected to subsequent processes described below without special safeguards.

As shown in figure 1, the next step consisted of spinning the photoresist S1813 on the Cu surface followed by a soft-baking process on a 90 °C hot plate for 2 min. The designed mask was printed in positive with a high-resolution laser writer (Heidelberg Instruments DWL66, Conversion Software V8.65) on a mask glass wafer for lithography. The S1813 photoresist applied on the Cu surface was patterned with a mask aligner (HTG System III Contact Aligner) using an exposure time of 14 s with a wavelength band of 365–405 nm (measured intensity 14 mW cm^{-2} at 365 nm), and subsequently developed in AZ 300 MIF developer for 2 min. To improve mask stability, adhesion and chemical resistance, a hard bake was performed for 10 min at 120°C.

The wafer with copper foil was then dipped into the copper etchant at room temperature, which is a commercial mix of 30% $FeCl_3$ +3% HCl +67% H_2O. One of the reactions for etching of copper with ferric chloride is

$$Cu_{(s)} + 2Fe^{3+} + 3Cl^- \rightarrow CuCl_3{}^- + 2Fe^{2+}. \quad (1)$$

Other chloride complexes are also formed. The Fe^{3+} ions are reduced to Fe^{2+}, which remain in solution, while the copper metal is oxidized to Cu^{2+}. HCl assists in the dissolution of the ferric chloride, and also etches copper itself. Wet etching is a three-phase dynamic system, which will be discussed later.

Next, the copper foil GDM was released using a lift-off process in acetone, and was then thoroughly rinsed with deionized water and dried. Each finished piece was held between wafers for ease of handling.

The patterned mask and etched pattern were checked with an Olympus BX60/U-CFU real-time confocal microscope, which employs a newly developed slit method scanning disc that blocks defocused reflected light from samples and allows only focused light to pass. The U-CFU has excellent vertical detection; individual layers in a multi-layer wafer can be distinctly observed with this instrument. The pore dimensions were measured with an optical profilometer. A JSM-7400F field emission scanning electron microscope (FESEM) was used to check the cross section of the etched trench and small features with high spatial resolution.

3. Results

Etching is an exothermic process and the etching rate generally increases with temperature. Therefore, etching was performed at room temperature, in our case for better control. In wet isotropic etching, the etchant ideally removes the substrate at the same rate in all directions and produces a hemispherical trench. With mask etching, the typical etched trench is shown in figure 2. The dimensions of the trench are related to the etching rate and etching duration, as well as to the mask width, w_m. Considering our application and materials with very thin features, the study here only focused on the parameter of trench width, w_t. Accordingly, etching experiments were performed with mask diameters of 2, 3, 4, 5, 6, 7, 8, 10, 15 and 20 μm. Figure 3 shows the dependence of trench width and the average etching rate on the mask width. The lowest of the three curves (circles) corresponds to the etching rate, whereas the two upper curves correspond to the trench width after 20 min (diamonds) and 30 min (squares). It can be seen that both the trench width and the etching rates increase with mask width as expected,

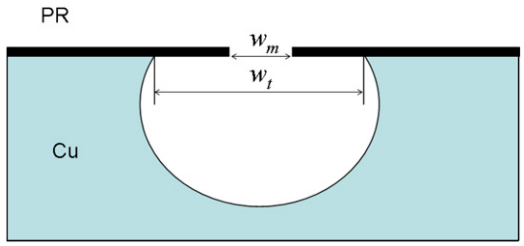

Figure 2. Typical cross section of the etched trench of copper.

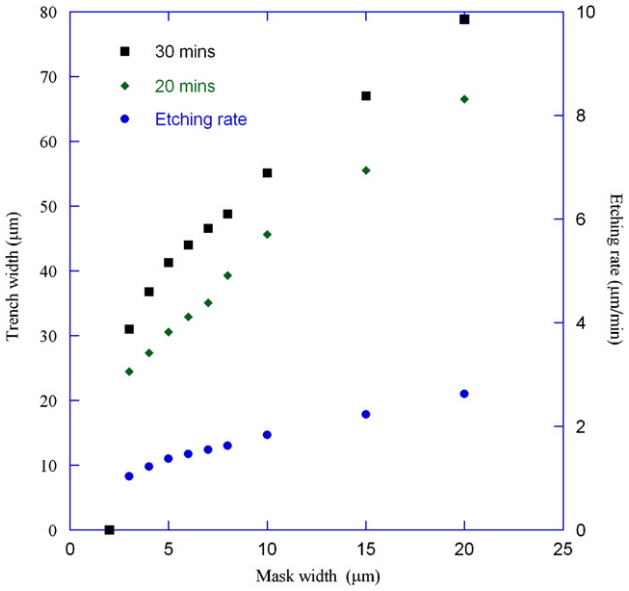

Figure 3. Dependence of trench width and etching rate on mask width.

when the mask width is greater than 2 μm. With a mask width of 2 μm, no etching was observed.

Wet etching is a three-phase dynamic system which typically involves the following steps (i) liquid-phase transport of the etchants from the bulk solution to the copper surface, (ii) reactions with the etchant on the surface of solid-phase copper that generates products in both the gas phase and the liquid phase and (iii) transport of products from the copper surface to the bulk solution. The transport of etchant through the mask can be modeled as transport in porous media, which is governed by the following equation:

$$\Delta p = -\frac{4\gamma \cos\theta}{w_t}, \tag{2}$$

where γ is etchant surface tension, θ is contact angle of etchant on photoresist S1813 and Δp is the pressure head needed to penetrate etchant through the mask with the width of w_t. A smaller mask width requires a larger pressure head. For the pressure head used in our study, the limiting value of w_t was 2 μm, below which the etchant failed to penetrate through the mask and no reaction occurred. Reducing the hydrophobicity of mask photoresist or increasing pressure head will enable the use of even smaller mask widths.

After the etchant passes through the mask and reaches the copper surface, the reaction rate is controlled by a combination of mass-transport rates and chemical kinetics. When the mass transport and kinetic resistances are comparable in magnitude, both of them will affect the rate of etching. However, in micro-scale masked etching, the generation rate of products gradually exceeds their exit rate through the mask pore with increasing trench size. Consequently, mass-transport resistance dominates the etching process and the overall etching rate is mainly affected by the mask width [14]. Increasing the mask width results in larger etching rate due to the reduction of the effective mass-transport resistance. The average etching rates here ranged from 1.03 μm min^{-1} to 2.36 μm min^{-1} with mask widths varying from 3 to 20 μm.

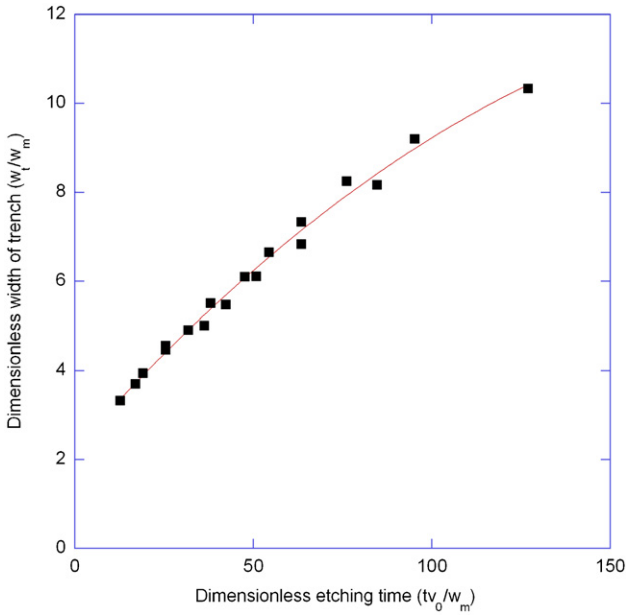

Figure 4. Dimensionless etched width with non-dimensional etching time.

Figure 4 shows the results of the trench width and etching time for different cases. The trench width w_t is normalized by the mask width, w_m, while the dimensionless etching time is expressed as tv_0/w_m. Here v_0 is the standard etching rate at the temperature of 50 °C, and its value is 12.7 μm min^{-1}. The excellent collapse of data in figure 4 validates our non-dimensionalization scheme. As expected, the dimensionless trench width (w_t/w_m) increases with dimensionless time. However, the etching rate gradually reduces with dimensionless etching time, which agrees well with results shown in figure 3. Note that the smallest dimensionless etching time corresponds to the largest mask width. The data in figure 4 have been curve fitted with a second-order polynomial (indicated by the solid line):

$$\frac{w_t}{w_m} = 2.25 + 0.09\left(\frac{t}{w_m}v_0\right) - 2.0\times 10^{-4}\left(\frac{t}{w_m}v_0\right)^2. \tag{3}$$

The above equation can be used to predict the trench width and etching rate of copper (1 1 0) substrate, which has been sparsely investigated [13].

Various shapes of mask openings have also been examined including circles, squares, triangles, ellipses and rectangles. Figure 5 presents images, which were taken after 20 min of etching. The mask patterns of circle, triangle, square and ellipse are visible at the center of the images depicted in figures 5(*a*)–(*d*), respectively. It can be seen that the etched

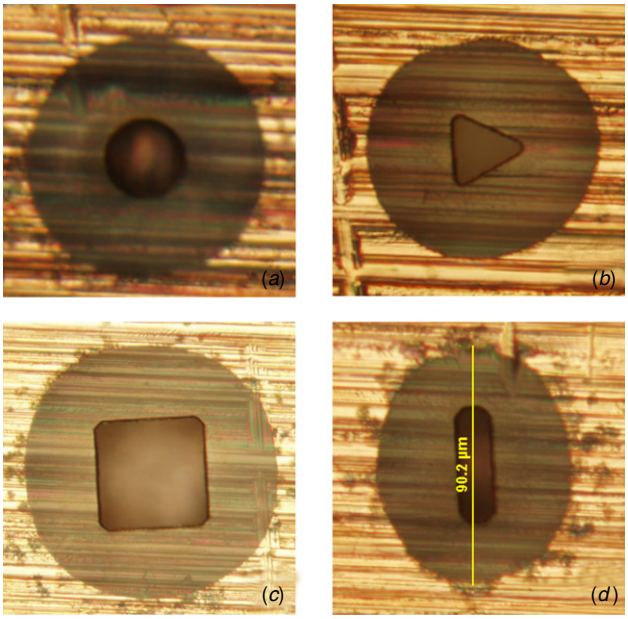

Figure 5. Effect of mask shape on isotropic copper etching.

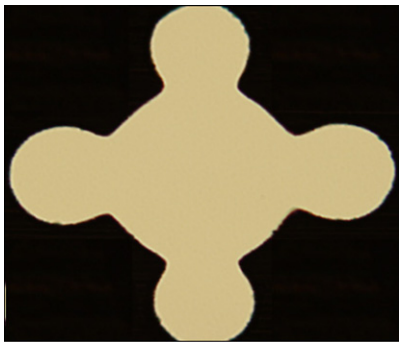

Figure 6. Non-circular shape obtained by designing the mask pattern.

trench shape in the first three cases gradually evolves to a relatively similar circular shape. This is attributed to the nature of wet isotropic etching and uneven ratio of mass-transport rates and chemical kinetics, which were discussed in the previous section. Consequently, the initial mask shape is 'forgotten' at long etch times. In the case of figure 5(*d*), it is observed that even increasing the aspect ratio of mask shape within a certain range does not significantly affect the final etched pattern when the etching duration was of the order of 10 min. Larger aspect ratios result in bigger pore dimensions, which are not preferred in our application. Because non-circular pore shapes will be beneficial for two-phase transport through the GDM, we attempted to create such pores by careful pattern design while maintaining the same etching time. An example of one such image is shown in figure 6. The configuration of two-phase transport in the pores is characterized by the pore geometry, surface tension of the fluid, the capillary pressure and the wettability of pore walls. Pure liquid water cannot be imbibed and will not penetrate into a pore with hydrophobic surface property (contact angle $>90^{\circ}$) without sufficient capillary pressure, which is defined

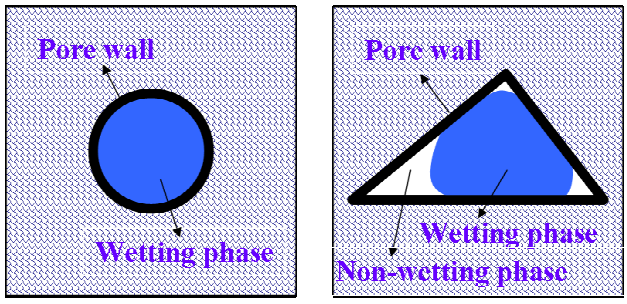

Figure 7. Comparison of capillary action through circular and non-circular hydrophobic pores.

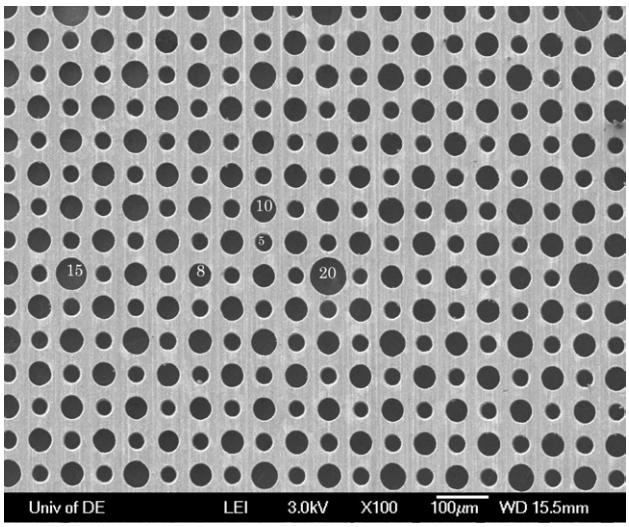

Figure 8. Typical image after etching.

by a relation similar to equation (2). Figure 7 shows the comparison of two-phase configurations through circular and non-circular hydrophobic pores. For a capillary with a circular pore the liquid water fills the entire pore, while in the non-circular case the liquid water occupies only a portion of the pore allowing passage of the gas through the open region at the same time. The latter mechanism allows GDM to transport the reactants in and the products out from partially covered pores and reduce flooding in the fuel cell.

Based on the above results, mask widths of 5, 8, 10, 15 and 20 μm were chosen for our application. Figure 8 shows a SEM image of the copper GDM after 20 min of etching. The number inside the pore indicates the mask width in μm. The number density of mask widths of 20, 15, 10, 8 and 5 μm relative to the number density at 20 μm is 1, 1, 8, 54 and 64, respectively. The mean pore size after etching for 20 min is 35.65 μm, while the porosity of the copper GDM is about 21%. It should be noted here that the mean pore size and porosity could be changed by altering the mask width, varying the etching time and changing the number density ratio of the pores.

4. Conclusions

A new technique to fabricate gas diffusion media for PEM fuel cell application from copper foil with improved thermal

and electrical conductivities has been demonstrated. More importantly, the technique with mask-patterned isotropic etching allows us to control the pore dimensions, porosity and pore size distributions, which are important features of the GDM in a fuel cell. The fabrication of super thin copper foil and the influence of mask width and mask shape on trench width, etching time and etching rate have been investigated. With micro-feature masked etching, the etching rates, which are about 1–2 μm min^{-1} are mainly dominated by mask widths due to mass-transport resistance. A correlation to predict trench width with etching time was derived; normalizing by mask width allows for excellent collapse of the data. This technique should prove useful in designing the next generation of GDMs for fuel cell applications.

Acknowledgments

This work was supported by the Federal Transit Administration (grant FTA JPP-05-DE-03-7001). A portion of this work was performed at the Cornell Nanoscale Science & Technology Facility, a member of the National Nanotechnology Infrastructure Network which is supported by the National Science Foundation (grant ECS 03-35765).

References

[1] Demirdöven N and Deutch J 2004 *Science* **305** 974–6
[2] Mathias M F, Roth J, Fleming J and Lehnert W 2003 *Handbook of Fuel Cells—Fundamentals, Technology and Applications* vol 3, ed W Vielstich, A Lamm and H A Gasteiger (New York: Wiley) pp 517–37
[3] Lee W K, Ho C H, Van Zee J W and Murthy M 1999 *J. Power Sources* **84** 45
[4] Lin G and Nguyen T V 2005 *J. Electrochem. Soc.* **152** A1942
[5] Zhang F Y, Yang X G and Wang C Y 2006 *J. Electrochem. Soc.* **153** A225–32
[6] Passalacqua E, Squadrito G, Lufrano F, Patti A and Giorgi L 2001 *J. Appl. Electrochem.* **31** 449
[7] Benziger J, Nehlsen J, Blackwell D, Brennan T and Itescu J 2005 *J. Membr. Sci.* **261** 98–106
[8] Hamada A and Nakato K 2005 *US Patent* 6899971
[9] Ho C-M and Tai Y-C 1998 *Annu. Rev. Fluid Mech.* **30** 579–612
[10] Williams K R and Muller R S 1996 *J. Microelectromech. Syst.* **5** 256–69
[11] Yen S C, Chen Y H, Kuo J S and Huang J H 2006 *Meet. Electrochem. Soc.* **501** 37
[12] Phillips J R, Griffis D P and Russell P E 2000 *JVSTA* **18** 1061
[13] Kondo K, Kurihara H and Murakamia H 2006 *Electrochem. Solid-State Lett.* **9** C36–7
[14] Nilsson D, Jensen S and Menon A 2003 *J. Micromech. Microeng.* **13** S57–61